GROUND VIBRATION TESTING OF A HIGH ASPECT RATIO WING WITH REVOLVING CLAMP

Gabriele Dessena[1], Dmitry I. Ignatyev[1], James F. Whidborne[1], Alessandro Pontillo[2] & Luca Zanotti Fragonara[1]

[1]School of Aerospace, Transport and Manufacturing, Cranfield, Bedfordshire, MK43 0AL, UK
[2]Department of Aerospace Engineering, University of Bristol, Bristol, BS8 1QU, UK

Abstract

The advancements in the aeronautical industry and research on materials and manufacturing methods in the last 70 years have been shifting the paradigm of wing design to high aspect ratio flexible wings. These wings can show a varying behaviour in different operating conditions, as per the nature of their geometry and materials. This work proposes a case study of a high aspect ratio flexible wing in order to study the effect of operating conditions on its structural properties. To test different operating conditions on the ground, a revolving clamp is designed to attach the specimen to a clamp-on shaker. A clear relationship between the wing's modal properties, and so structural properties, and the angle the clamp sets is found.

Keywords: Experimental Modal Analysis, Ground Vibration Testing, High Aspect Ratio, Structural Dynamics, Flexible Wing

1. Introduction

During flight operations an aircraft is subject to multiple external factors, from loads to environmental conditions. Estimating the complete behaviour of a flexible high aspect ratio (HAR) wing in such environment is not a trivial task and involves careful modelling and testing to ensure compliance with regulations. This work aims to discover the relationship between the change in environmental conditions and structural properties by modal analysis, in particular by detecting the induced change on the modal parameters. For this, a revolving clamp for a clamp-on shaker was designed, the clamp allows to change the setting angle (α_{gvt}) of a HAR wing while on the shaker and to run ground vibration testing (GVT) of the wing at different α_{gvt}s. In this sense, the change in the α_{gvt} of the clamp is meant to simulate, on the ground, the wing's deflection by inducing different deformations on the specimen thanks to the altered influence of gravity. The specimen used in this testing campaign is a wing from Cranfield University's Beam Reduction and Dynamic Scaling (BeaRDS) project [1, 2, 3, 4], which is a HAR flexible wing, made of aluminium, stainless steel, and 3D printed plastics, developed as a dynamically scaled model of a narrow body civil jet airliner and known as eXperimental BeaRDS 2 (XB-2). Within this work, only the vertical and torsional displacements are considered and, particularly, the first three modes' modal parameters, where vertical displacement is dominant, are extracted.

The experimental setup and its results are the focus of this work, which also includes some reference to the future use of the generated data.

The increasing awareness for the need of a greener aviation and the promise of lighter and more efficient structures is pushing a new paradigm in wing design: flexible HAR wings. Not only is this revolution focusing on the design, but, as a process that started more than 70 years ago, also on materials. In fact, new ultralight and customisable composite materials are the enabling technology [5] of the modern configurations. However, all these ingredients create a reduction in stiffness and modal frequencies of the structure, causing a decrease in aeroelastic phenomena onset speeds,

which if overlooked, can create several, even catastrophic [6], problems. Nevertheless, the designers have two main instruments in their hands to prevent these occurrences: GVT and finite element modelling (FEM). The former is the main focus of this work.

In aeronautics, the term GVT replaces the term Experimental Modal Analysis and the most common targets of GVT are the whole craft [7], wings [8] and helicopter blades [9]. The main purposes of GVT in aeronautics is to update, or validate, the specimen's finite element model (FEM) [10, 11], which in turn can be used to characterise the aeroelastic onset speeds [7]. These objectives are usually obtained by extracting the modal parameters, namely natural frequencies (ω_n), damping ratios (ζ_n), and mode shapes (ϕ_n), from the experimental data [7, 12, 13]. However, for flexible wings, sometimes, more involved testing techniques have to be employed in order to characterise some particular response of the wing, such as damping [14] or non-linearities [15]. Nevertheless, a band-limited random verification is sufficient to achieve the goal of this work [16]. The mean for extracting modal parameters are system identification (SI) techniques [17] which create a model from the measured data, which can be in two domains: time and frequency. Depending on the domain, some SI methods are preferred over other, such as numerical algorithms for subspace state space system identification in time domain and least-squares complex exponential, or rational fractional polynomial, in the frequency domain. For the purpose of this work a frequency domain technique, the Loewner Framework (LF), recently introduced by some of the authors for mechanical systems [18, 19, 20] is the method of choice.

The remainder of this work is structured as follows. In Section 2, the specimen, the clamp, and the experimental setup are discussed in detail and in Section 3 The results are outlined and, finally, in Section 4 the conclusions and future works are presented.

2. Methods

In this section the specimen tested, the XB-2 wing, and its motivation are introduced. In addition, the revolving clamp design and mechanism are explained prior to describing the experimental setup and the data collection and processing procedure.

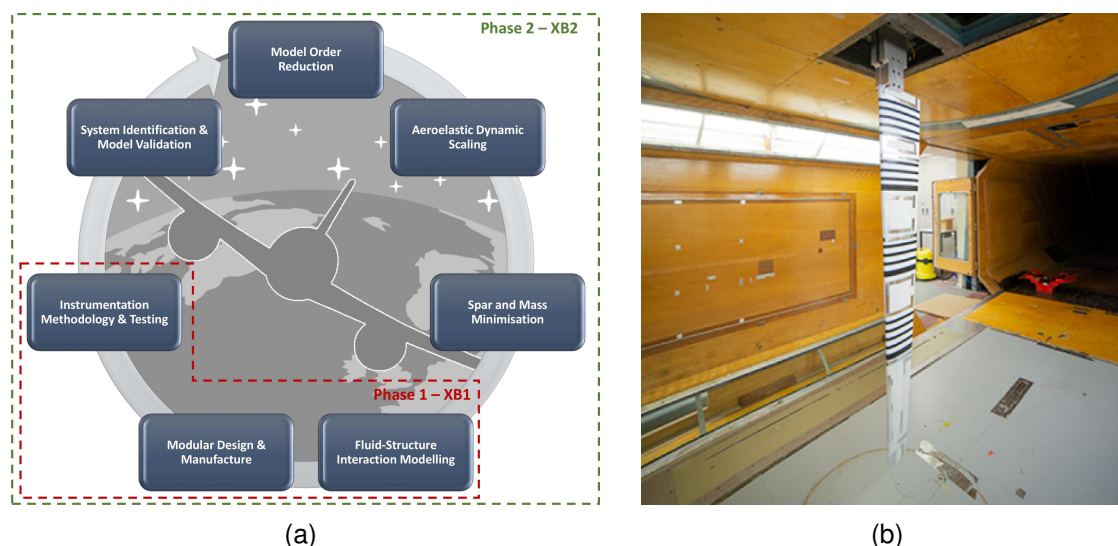### 2.1 Beam Reduction and Dynamic Scaling High Aspect Ratio Wing

(a)   (b)

Figure 1 – BeaRDS work flow (retrieved from [1]) and XB-2 in the 8'x6' Cranfield University wind tunnel (retrieved from [4]).

The BeaRDS framework, Figure 1a, was a project from Cranfield University which aimed to create a work flow for the design, testing and modelling of flexible wings based on dynamically scaled prototypes. For the scope of validating the framework, the XB-2 HAR wing was designed and manufactured to be tested in the Cranfield University's 8'x6' wind tunnel. The wing has 4 main parts: the main spar, the stiffening tube, the added masses and skin. Since the only purpose of the masses

was for the dynamic scaling of a narrow body civil airliner [2] and, so, outside the scope of this study, they were removed for this round of testing.

XB-2's spar is machined out of two 6082-T6 Aluminium blocks and the tube and the linkages are made out of stainless steel, while the skin is made of strips of 3D printed Digital-ABS [21] and Agilus 30 [22], a rubber-like material. In the skin, the Agilus 30 black strips, in Figure 1b, alternate the white Digital ABS sections, allowing the skin to flex considerably and retaining structural continuity. Notably the wing's skin is printed in only three sections thanks to Polyjet technology [23] that allows for the use of different materials within the same print. Table 1 recaps the materials properties of interest.

Table 1 – Materials' properties.

Material	Young Modulus [GPa]	Poisson Ratio [-]	Density [kgm^{-3}]
6082-T6 Aluminium	70	0.33	2700
Stainless Steel	193	0.33	8000
Digital ABS	2.6-3.0	0.33[24]	1170-1180
Agilus 30	NA	NA	1140

Figure 2 – The spar and tube assembly (retrieved from [8]).

The torque box of the wing is made of the spar and tube assembly, in Fig. 2, and it is responsible to carry the loads transferred from the skin. The mass of the spar and tube assembly is 1.362 kg. The spar was machined from two separate aluminium blocks, welded at mid-span and secured with a set of four I-plates bolted to the two sub-parts to ensure continuity. The spar features a Saint George's cross-like cross section, which changes proportions linearly along the span, and a rectangular cross section in the root section, which is used as a clamping point by the revolving clamp. The overall length of the spar is 1.45 m, while the suspended span when clamped is 1.325 m.
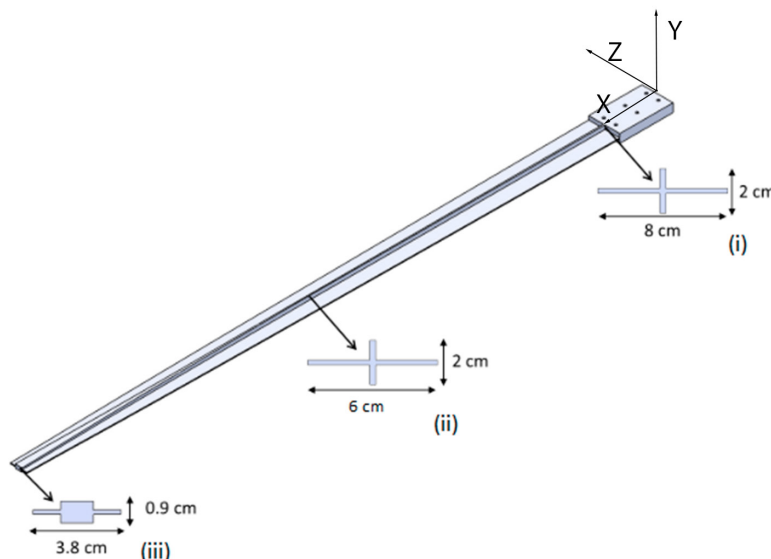

Figure 3 – Spar's CAD model with section view at the location of interest: (i)root, (ii)mid-span, and (iii)tip (adapted from [2]).

Three positions within the clamp define the cross section, (i) the root, (ii) the mid-span, and (iii) the tip, whose shapes are shown in Figure 3. The tube, having an outer diameter of 10 mm, a thickness of 1 mm and being 550 mm long is connected to the spar at three points and is located aft of the spar and was added to improve bending and torsional stiffness. The complete wing assembly comprising

spar, tube, and skin weights 3.024 kg and has a overall span of 1.5 m featuring a root chord of 236 mm and a tip chord of 83 mm with a leading edge (LE) sweep of 14.9°. The reader interested in a more profound review of BeaRDS and the specimen is referred to [1, 2, 3, 4, 8, 20], while Table 2 recaps XB-2's physical properties.

Table 2 – XB-2 wing properties

Property	Details	Unit
Semi span	1.5	m
Root chord	236	mm
Tip chord	83	mm
LE sweep	14.9	°
Mass	3.024	kg

2.2 The Revolving Clamp

This work is based on the possibility of running GVT of the XB-2 wing at different α_{gvt}s. Hence, a suitable device had to be designed and the revolving clamp, in Fig. 4a, was conceived.

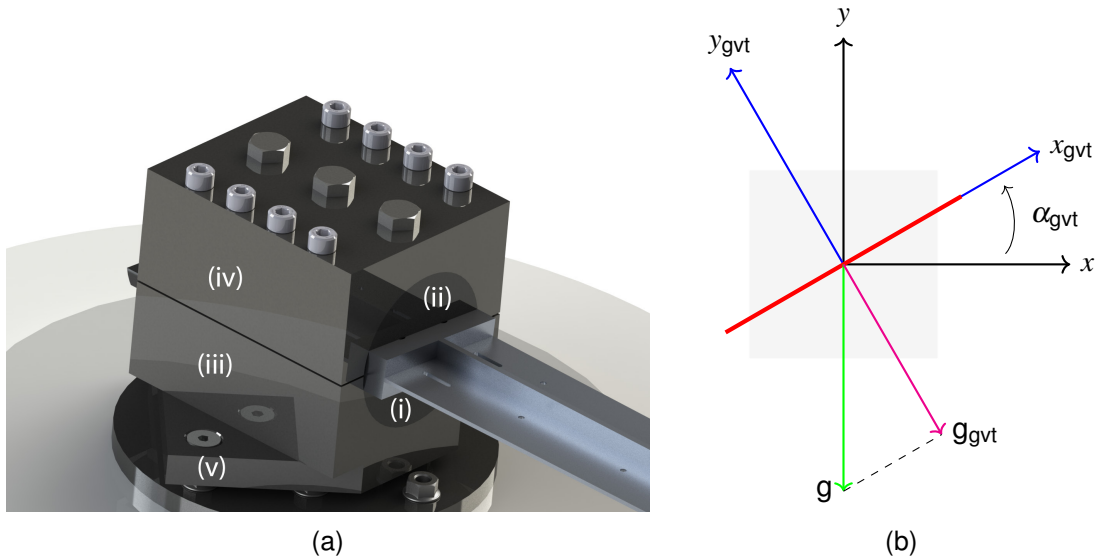(a)   (b)

Figure 4 – Figure 4a shows the rendering of the revolving clamp mounted on the shaker with labelled parts: (i) the lower sock, (ii) the upper sock, (iii) the lower end, (iv) the upper end, and (v) the base plate. A schematic demonstrating the effect of α_{gvt} over gravity loads on the specimen is shown in Figure 4b.

The clamp consists of five parts: (i) the lower sock, (ii) the upper sock, (iii) the lower end, (iv) the upper end, and (v) the base plate. The lower and upper sock are clamped directly to the wing's root using four M6 cap head socket bolts, then the two socks and the specimen are secured between the lower and upper end. The lower end is directly bolted to the base plate with three M8 socket countersunk bolts and serves as an adaptor for the fixings on the shaker and is secured to it with seven M8 socket countersunk bolts. The upper end clamps the specimen to the lower end clamp with 8 M8 cap head socket bolts, the four bolts at the corners are bolted to the lower end end clamp, while the four inboard to directly to the base plate. Finally, three M10 hexagonal bolts are placed in the upper clamp to further constrain the sock assembly from rotating or slipping. The specimen α_{gvt} is adjusted by untightening the bolts on the upper end clamp and setting the specimen to the required angle by placing an inclinometer over the extruded tab of the lower sock. The clamp, excluding the base plate, was machined from a single block of aluminium and its mass, excluding the fixings, is 3.583 kg. The fixings weight is 0.606 kg, giving a total mass of 4.189 kg.

The motivation behind the revolving clamp is to change the effect of gravity on the static configuration of the wing. In fact, the effective downward, normal to the wing inclination, effect of gravity decreases. This is clearly depicted in 4b, where the phenomenon is graphically described. The black axes are the global axis, while the blue axes are the local axis relative to the inclined wing and the red thick line identifies the wing's profile. The actual gravity vector g is the green arrow and the relative gravity on the inclined wing ($g_{\alpha_{gvt}}$) is the pink arrow. From simple trigonometry the relationship between the two is the following:

$$g_{\alpha_{gvt}} = g \times \cos(\alpha_{gvt}) \tag{1}$$

Summarising, the increase in the wing's inclination angle decreases g_{gvt} and so the wing's deflection from it's own weight.

2.3 Experimental Setup and Data Processing

The testing campaign involves the XB-2 wing at three different setting angles (α_{gvt}s): 0, 5, and 10°. The specimen is excited with a random vibration excitation at three different inputs for 20 min. However, only 18 min are considered while post-processing the data to exclude any transients.

Table 3 – Accelerometers specifications.

| ID #	Model	Sensitivity [mVg^{-1}]	Mass [g]
Accelerometers			
0	PCB Piezotronics® model: 356B18	995	25
1R	PCB Piezotronics® model: 356A16	96.5	7.4
1L	Isotron® accelerometer model 7251A	10.3	10.5
2R	PCB Piezotronics® model: 356A16	97.2	7.4
2L	Isotron® accelerometer model 7251A	10.08	10.5
3R	PCB Piezotronics® model: 356A45	100.2	4.2
3L	Isotron® accelerometer model 7251A	10.34	10.5
4R	Brüel & Kjær® accelerometer type 4507-002	94.12	4.8
4L	Brüel & Kjær® accelerometer type 4507-002	95.52	4.8
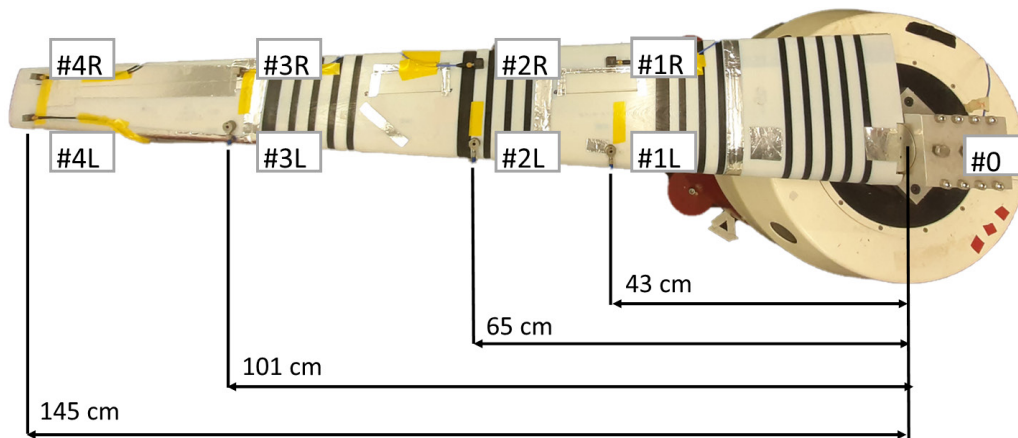
Figure 5 – Accelerometers locations (retrieved from [8]). Note that the accelerometers do not appear aligned due to the optical effect of the camera lens.

A Data Physics® Signal Force™ modal shaker controlled by its DP760™ close-loop control software, running on a consumer grade laptop, drives the specimen. Eight accelerometers are attached to the specimen and another on the clamp's lower sock, for feedback purposes. The accelerometer at the clamp is positioned in such a way to record the vertical acceleration normal to the wing inclination, this ensures that even at different amplitudes the shaker delivers the same output in the direction normal to the wing's direction. The accelerometers' span-wise locations are decided using a sensor placement routine based on a genetic algorithm[25]: a FEM model was employed as a baseline and a

genetic algorithm minimised the sum of the off-diagonal terms of the Auto-Modal Assurance Criterion (Auto-MAC) by changing the sensors position along the span. The accelerometer positions are shown in Fig. 5 and their characteristics in Table 3. The experimental setup is completed by a desktop machine that collects the data from a National Instruments cDAQ-9174, to which the accelerometers are connected, via a LabVIEW program, as shown in Figure 6.
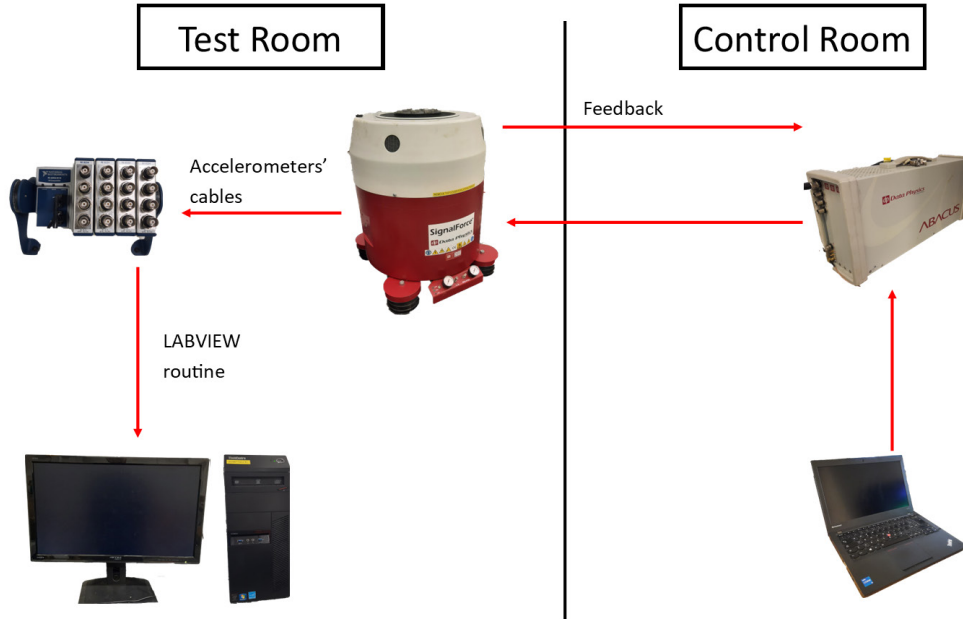

Figure 6 – Testing setup (retrieved from [8]).

The wing is excited with a random verification at different input amplitudes. The amplitudes are considered normal to the wing's inclination and are, from now on, always referred as Low, Medium, and High. They, relatively, correspond to 0.919, 0.649, and 1.590 RMS (Root mean square) ms^{-2}. To ensure the highest precision and repeatability, the tests are repeated 5 times for each input scenario at each α_{gvt} totalling 45 cases. The nine input and α_{gvt} cases are summarised in Table 4.

Table 4 – Test cases for the XB-2 wing considering input amplitude and α_{gvt}.

Case	Input	α_{gvt} [º]
1	Low	0
2	Medium	0
3	High	0
4	Low	5
5	Medium	5
6	High	5
7	Low	10
8	Medium	10
9	High	10

For all scenarios the random input signal is bandwidth limited between 2 and 100 Hz and lasts 20 min and was down-sampled to 256 Hz from the original sampling frequency (f_s) of 5120 Hz. Then, the Frequency Response Functions (FRFs) are generated by taking the Fast Fourier Transform of all time histories, relative to channel #1-8 and dividing them by the input, channel # 0. Prior to identification, the FRFs are smoothed with the MATLAB built-in function smoothdata by setting the moving average window length to 60.

3. Results and Discussion

In this section the results of the 45 independent cases are presented. First, a single case is deeply investigated in detail then the remaining cases are presented focusing in the relationship between α_{gvt}, input amplitude and modal parameters. In Figure 7, the FRFs for Case 1 are shown. All channels are superimposed for conciseness, showing the peaks of the first three vertical dominant modes. While only three modes are detected, within this work they are going to be referred as first, second, and fourth because it was found in a previous testing campaign [8] that a horizontal dominant mode can be found around 14 Hz.
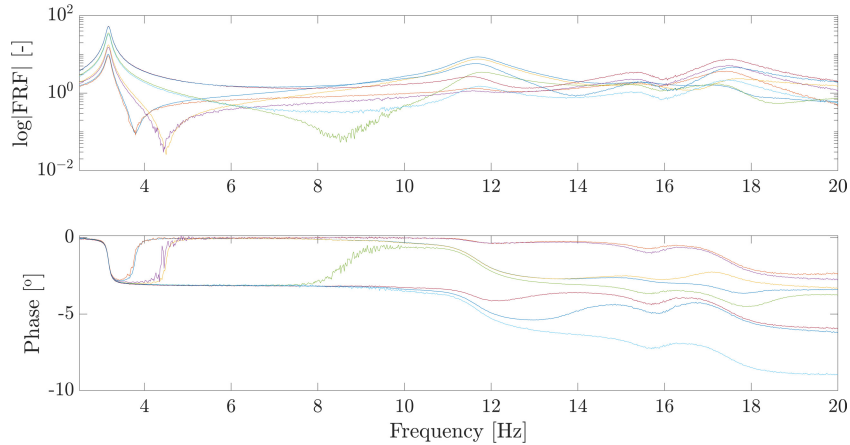
Figure 7 – Case 1: FRFs relative to channels #1-8 of of a single realisation of the low input 0° α_{gvt} case. All channels superimposed for conciseness.

The modal parameters are extracted via LF using a stabilisation diagram for the 45 instances and then the results of the five instances within the same case are averaged to obtain the modal parameters. Figure 8 shows the stabilisation diagram of the first instance for Case 1 and clearly shows the first three vertical dominant modes by superimposing the stable modes, between LF's order 6 and 200, to the FRFs relative to channels # 2, 4, 6, and 8. The modes are regarded as stable when the difference in ω_n (Δf) is within 1%, that of ζ_n is 10% and Modal Assurance Criterion (MAC) [26] value over 0.95 within the preceding ten.
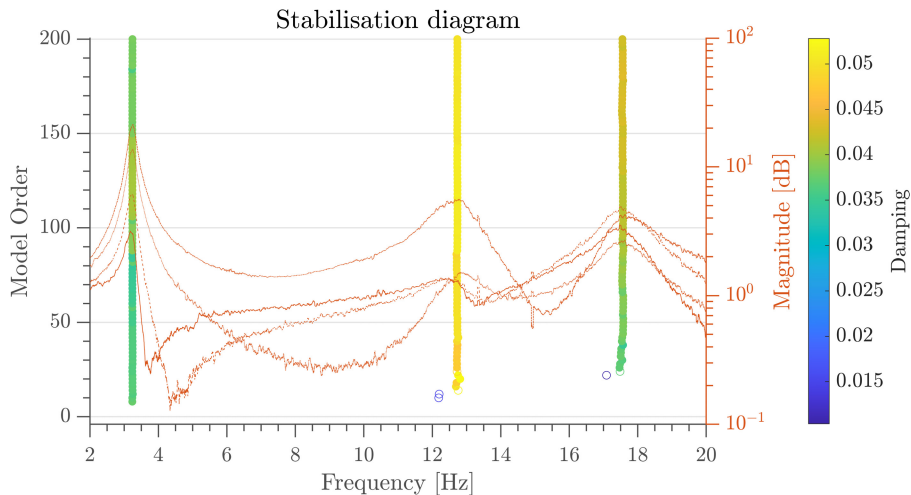

Figure 8 – Case 1, first instance: stabilisation diagram computed with the following parameters: $\Delta f = 1\%$, $\Delta \zeta = 10\%$ and $\Delta MAC = 0.95$.

In Table 5 the identified modal parameters, ω_n and ζ_n, of Cases 1, 2, and 3 are presented. As these cases refer to the same α_{gvt}, the decrease in ω_n over the increase in input amplitude shows that the wing, contrary to usual expectations for a beam-like structure, features a softening behaviour. On the other hand, ζ_n remains roughly constant for all inputs, only ζ_4 is considerably larger for Case 3.

Table 5 – Cases 1, 2, and 3: average value, over five instances, of natural frequency and damping ratio parameters.

Case	1		2		3	
Mode	ω_n	ζ_n	ω_n	ζ_n	ω_n	ζ_n
1st Bending	3.21	0.035	3.20	0.023	3.17	0.018
2nd Coupled	12.50	0.053	11.92	0.053	11.76	0.055
4th Coupled	17.36	0.045	17.15	0.045	17.05	0.057

For the same Cases taken under consideration in Table 5, Figure 9 shows $\phi_{1,2,4}$, which are superimposed to the baseline shape for a clearer visualisation.
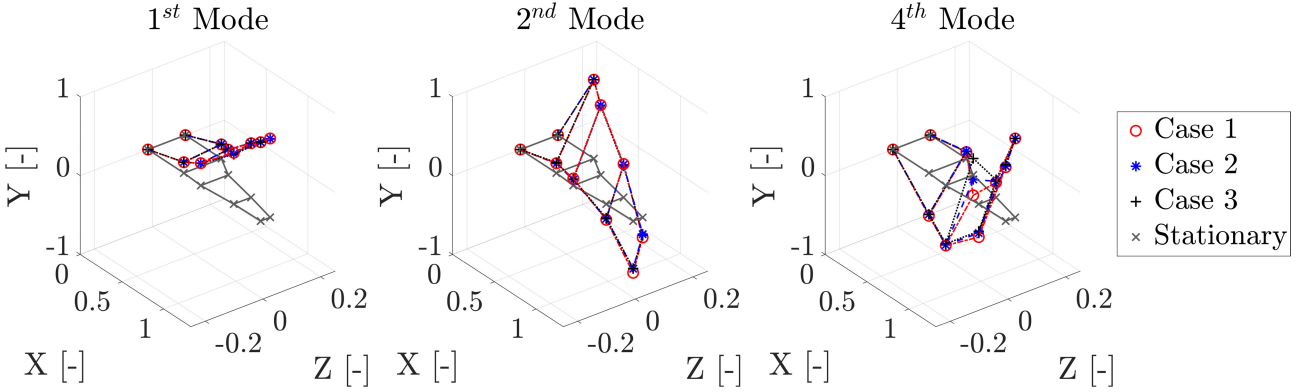
Figure 9 – Case 1, 2, and 3: mode shapes of the first three vertically dominant modes.

The result for first three cases, which take into consideration a $\alpha_{gvt} = 0^o$ and the three input levels, show that the structure's modal response is influenced by the input amplitude. In particular, the behaviour detected for this particular wing is softening, which means that as the input amplitude increases the ω_n decrease. This kind of behaviour is easily detectable [16] with the band-limited random verification of this series of test. As it is usually the case for lightly nonlinear structure, the ζ_n and ϕ_n are not massively influenced by the input amplitude. Nevertheless, the only difference concerning ϕ_n is found in the fourth mode, where the displacement linked to channel #3L fluctuates. Given the dependency of the modal response to input amplitude, the results for the nine cases under scrutiny are presented in a way that takes into consideration the different amplitudes. In Figure 10, first, Figure 10a, compares the ω_n for the low input amplitude, then, Figure 10b, those for the medium input and, finally, Figure 10c reports on the ω_n for the high input amplitude. The boxplots used reports the results for all 45 instances. In fact, for each case the median value is represented by a red line, the bottom and top blue edges of the box indicate the 25th and 75th percentiles and the whiskers the largest and smallest data points not considered outliers, while the red plus symbol indicates the outlier values. These give a statistical significance to the results and gives an indication of their trustworthiness. The boxplots are also accompanied by a regression line, in black, to highlight the ω_n trend in relation to α_{gvt}. For all the cases compared, exception made for the first mode at $\alpha_{gvt} = 5^o$ and high input amplitude, the ω_n decrease as α_{gvt} increases. While the results only consider structural effects, they follow the same trend of aero-structural theory [27]. In fact, an increase in natural frequencies is expected when flight speed increases. In the same way, when the setting angle is changed g_{gvt} is always smaller than g, as per Equation 1, and hence a smaller a deflection and ω_n are obtained.

The results for ζ_n are presented in the same way as per ω_n in Figure 11. Generally, damping ratios can be said to decrease over α_{gvt}, just as it is for ω_n. However, for a single instance, the second mode of the medium input scenario at $\alpha_{gvt} = 5^o$, this is not the case. Also, damping seems to be less influenced, without a clear trend, by the input amplitude. With the same consideration on gravity-induced deflection, the results are consistent from what is expected from theory [27] and experimental surveys [28] for a full wing.
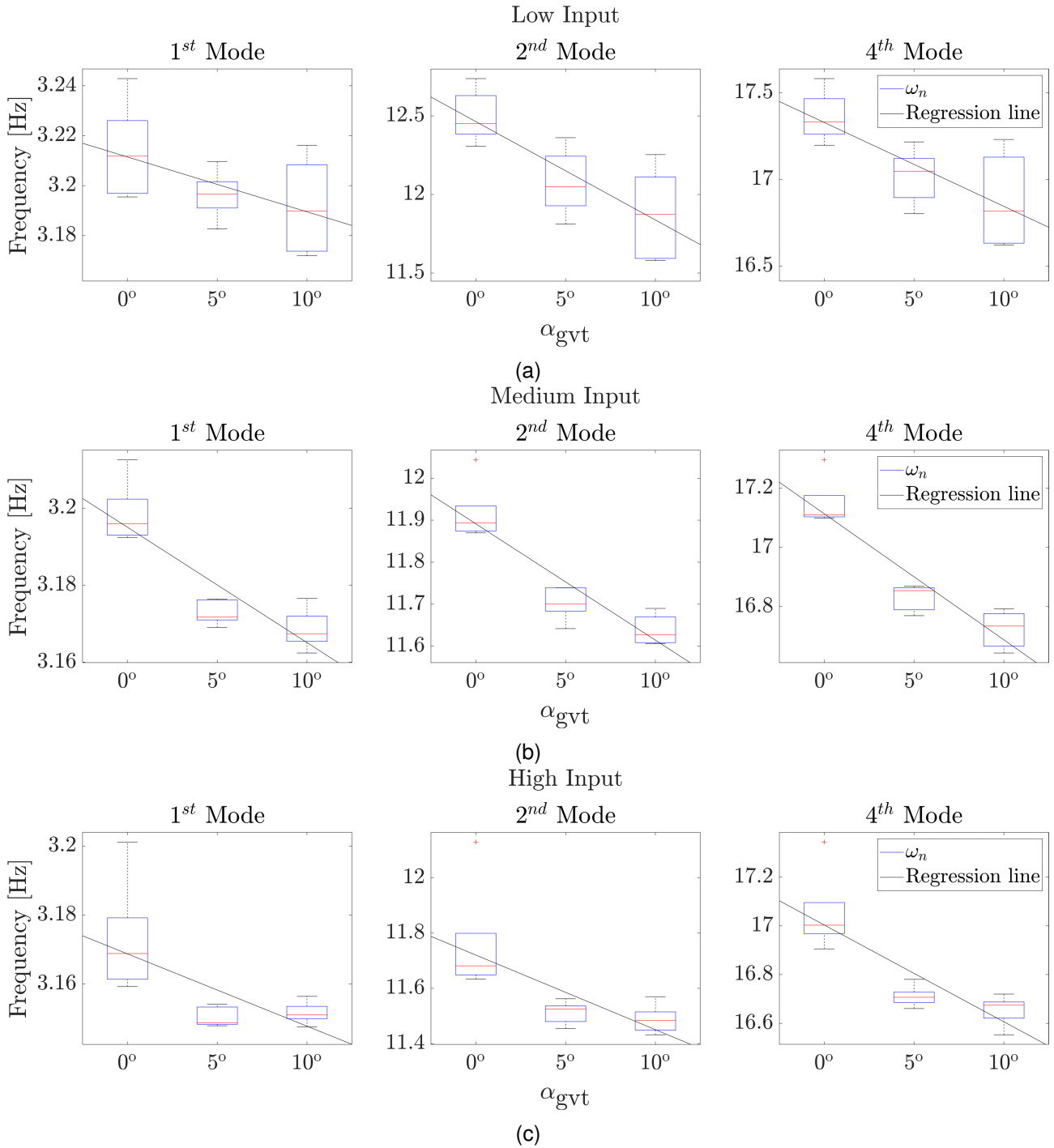
Figure 10 – Investigation on the effect of α_{gvt} on the natural frequencies. Figure 10a refers to the low input scenario, Figure 10b to the medium input and Figure 10c to the high input.

Lastly, the $\boldsymbol{\phi}_n$ are compared. Since a visual comparison of the all $\boldsymbol{\phi}_n$ for all cases is not efficient nor concise. Hence, the MAC value, relative to Case 1, is computed for the modes of all scenario. Only the diagonal terms of the MAC matrices are reported in Table 6, as the off-diagonal values are negligible. Since, the minimum value is found to be 0.85, it can be said that a good correlation exists between all respective $\boldsymbol{\phi}_n$ [12]. Notably, the third mode's correlation slightly diminishes for all cases. In fact this is true for Cases 1-3 as well. By inspection of Figure 9, it is trivial to detect a discrepancy at the channel #3L's position. This happens for the remaining cases as well and more notably for the highest input amplitude. However, all the respective modes are sufficiently correlated and no major variation is evident in their trajectories when compared.
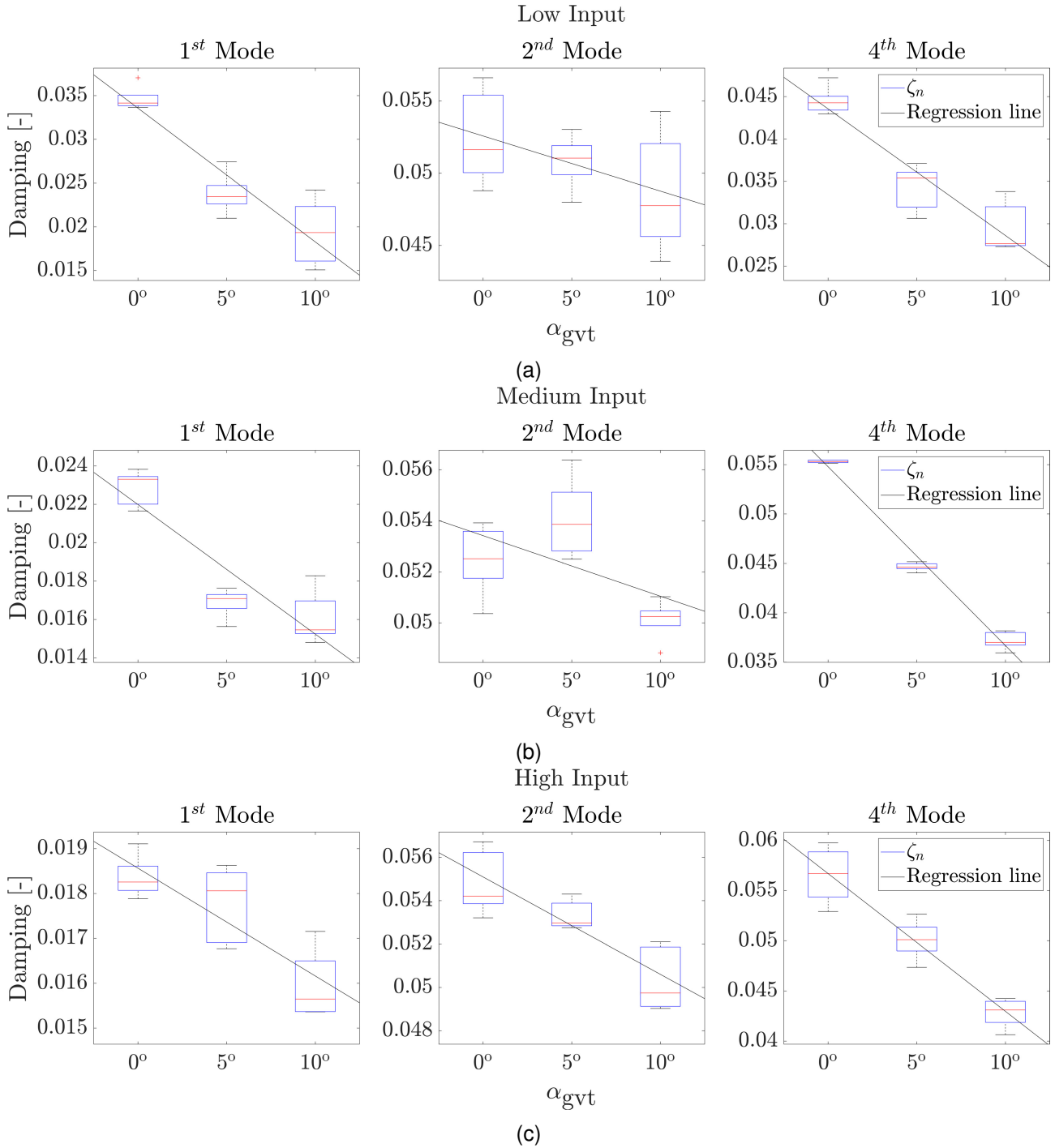
Figure 11 – Investigation on the effect of α_{gvt} on the damping ratios. Figure 11a refers to the low input scenario, Figure 11b to the medium input and Figure 11c to the high input.

Table 6 – Diagonal value of the MAC matrices between the computed mode shapes of Case 1 and all other cases.

MAC Value [-]							
	Mode				Mode		
Case	1st	2nd	4th	Case	1st	2nd	4th
2	1	1	0.98	6	1	1	0.85
3	1	1	0.91	7	1	1	0.99
4	1	1	1	8	1	1	.99
5	1	1	1	9	1	1	.91

4. Conclusions and Future Works

In this work, a high aspect ratio flexible wing undergoes ground vibration testing at three different inclination angles and input amplitudes on a revolving clamp to asses the relationship between the setting angle and its modal properties. A total of 45 test is run, which includes 5 instances for each setting angle and amplitude scenario. The modal parameters are extracted with the Loewner Framework, a technique recently introduced for mechanical systems by some of the authors, via stabilisation diagrams up to order $k = 200$. The five instances available for each case give a statistical significance to the results and ensure the meeting of repeatability requirements.

From the results, a clear relationship between the setting angle and modal parameters, particularly natural frequencies and damping ratios emerges. This has a direct link to the wing's stationary deflection, linked to gravity, whose effect decreases inversely to the setting angle. Both natural frequencies and damping ratios are found to decrease as the setting angle increases indicating that a greater stationary deflection is proportional to an increase in those quantities. Also, it was found that the wing shows a softening behaviour: the natural frequencies decrease as the input amplitude increases. Moreover, it is shown that the mode shapes are pretty much unchanged when the setting angle is changed, but, particularly the fourth mode, it is influenced by input amplitude, . These relationships can be used to build a wing's finite element model to study its aeroelastic properties and also to assess the feasibility of this testing procedure to, or in part, substitute, when paired with computational fluid dynamics techniques, wind tunnel testing for flutter and divergence onset speeds characterisation.

Contact Author Email Address

mailto:gabriele.dessena@cranfield.ac.uk

Funding

Acknowledgments

Copyright Statement

References

[1] A. Pontillo, D. Hayes, G. X. Dussart, G. E. Lopez Matos, M. A. Carrizales, S. Y. Yusuf, and M. M. Lone, "Flexible high aspect ratio wing: low cost experimental model and computational framework," in *2018 AIAA Atmospheric Flight Mechanics Conference*. Kissimmee, FL: American Institute of Aeronautics and Astronautics, 2018, pp. 1–15.

[2] S. Y. Yusuf, A. Pontillo, S. Weber, D. Hayes, and M. Lone, "Aeroelastic scaling for flexible high aspect ratio wings," in *AIAA Scitech 2019 Forum*. Kissimmee, FL: American Institute of Aeronautics and Astronautics, 2019, pp. 1–14.

[3] D. Hayes, A. Pontillo, S. Y. Yusuf, M. M. Lone, and J. Whidborne, "High aspect ratio wing design using the minimum energy destruction principle," in *AIAA Scitech 2019 Forum*. Kissimmee, FL: American Institute of Aeronautics and Astronautics, 2019.

[4] A. Pontillo, "High Aspect Ratio Wings on Commercial Aircraft: a Numerical and Experimental approach," PhD thesis, Cranfield University, 2020.

[5] S. Malik, S. Ricci, and L. Riccobene, "Aeroelastic analysis of a slender wing," *CEAS Aeronautical Journal*, vol. 11, no. 4, pp. 917–927, 2020.

[6] T. E. Noll, S. D. Ishmael, B. Henwood, M. Perez-Davis, G. C. Tiffany, J. Madura, M. Gaier, J. M. Brown, and T. Wierzbanowski, "Technical findings , lessons learned , and recommendations resulting from the helios prototype vehicle mishap," in *UAV Design Processes / Design Criteria for Structures. Meeting Proceedings RTO-MP-AVT-145, Paper 3.4*, Neuilly-sur-Seine, France: RTO, 2007, pp. 3.4–1 – 3.4–18.

[7] C. R. Pickrel, "Airplane ground vibration testing - Nominal modal model correlation," *Sound and Vibration*, vol. 36, no. 11, pp. 18–25, 2002.

[8] G. Dessena, D. I. Ignatyev, J. F. Whidborne, A. Pontillo, and L. Zanotti Fragonara, "Ground vibration testing of a flexible wing: A benchmark and case study," *Submitted to [Aerospace]*, 2022.

[9] S. Weber, T. Kissinger, E. Chehura, S. Staines, J. Barrington, K. Mullaney, L. Z. Fragonara, I. Petrunin, S. James, M. Lone, and R. Tatam, "Application of fibre optic sensing systems to measure rotor blade structural dynamics," *Mechanical Systems and Signal Processing*, vol. 158, p. 107758, 2021.

[10] B. Sharqi and C. E. Cesnik, "Finite Element Model Updating for Very Flexible Wings," in *AIAA SCITECH 2022 Forum*. San Diego, CA: American Institute of Aeronautics and Astronautics, 2022, pp. 1–23.

[11] G. Dessena, D. I. Ignatyev, J. F. Whidborne, and L. Zanotti Fragonara, "A Kriging Approach to Model Updating for Damage Detection," in *EWSHM 2022*, lnce 254 ed., P. Rizzo and A. Milazzo, Eds. Singapore: Springer, 2023, ch. 26, pp. 245–255.

[12] D. J. Ewins, *Modal Testing Theory, Practice and Application*, 2nd ed. Baldock, UK: Research Studies Press, 2000.

[13] C. R. Pickrel, "A practical approach to modal pretest design," *Mechanical Systems and Signal Processing*, vol. 13, no. 2, pp. 271–295, 1999.

[14] M. Civera, S. Grivet-Talocia, C. Surace, and L. Zanotti Fragonara, "A generalised power-law formulation for the modelling of damping and stiffness nonlinearities," *Mechanical Systems and Signal Processing*, vol. 153, p. 107531, 2021.

[15] M. Civera, L. Zanotti Fragonara, and C. Surace, "An experimental study of the feasibility of phase-based video magnification for damage detection and localisation in operational deflection shapes," *Strain*, vol. 56, no. 1, pp. 1–19, 2020.

[16] K. Worden and G. R. Tomlinson, *Nonlinearity in Structural Dynamics Detection, Identification and Modelling*. Bristol, UK: Institute of Physics Publishing, 2001.

[17] L. Ljung, *System Identification: Theory for the User*, 1st ed. Englewood Cliffs, NJ: P T R Prentice Hall, 1987.

[18] G. Dessena, M. Civera, L. Zanotti Fragonara, D. I. Ignatyev, and J. F. Whidborne, "A Loewner-based system identification and structural health monitoring approach for mechanical systems," *Under Review [Structural Health Monitoring]*, p. 17, 2022.

[19] G. Dessena, M. Civera, D. I. Ignatyev, J. F. Whidborne, and L. Zanotti Fragonara, "On the accuracy and computational efficiency of the Loewner Framework for mechanical systems," *in preparation*, 2022.

[20] G. Dessena, M. Civera, A. Pontillo, D. I. Ignatyev, J. F. Whidborne, and L. Zanotti Fragonara, "Novel Modal Parameters Extraction Methods for Aeronautical Structures," *in preparation*, 2022.

[21] Stratasys, "Digital ABS plus," 2021. [Online]. Available: https://www.stratasys.com/it/materials/search/digital-abs-plus

[22] ——, "Agilus 30," 2021. [Online]. Available: https://www.stratasys.com/materials/search/agilus30

[23] N. P. Macdonald, J. M. Cabot, P. Smejkal, R. M. Guijt, B. Paull, and M. C. Breadmore, "Comparing Microfluidic Performance of Three-Dimensional (3D) Printing Platforms," *Analytical Chemistry*, vol. 89, no. 7, pp. 3858–3866, 2017.

[24] A. J. Keane, A. Sóbester, and J. P. Scanlan, *Small Unmanned Fixed-wing Aircraft Design*. Chichester, UK: John Wiley & Sons, 2017.

[25] A. Schulze, J. Zierath, S.-E. Rosenow, R. Bockhahn, R. Rachholz, and C. Woernle, "Optimal sensor placement for modal testing on wind turbines," *Journal of Physics: Conference Series*, vol. 753, no. 7, p. 072031, 2016.

[26] R. J. Allemang and D. L. Brown, "A correlation coefficient for modal vector analysis," in *Proceedings of the 1st International Modal Analysis Conference*. Orlando: Union Coll, 1982, pp. 110–116.

[27] J. R. Wright and J. E. Cooper, *Introduction to Aircraft Aeroelasticity and Loads*. Chichester, UK: John Wiley & Sons, 2014.

[28] I. Tsatsas, A. Pontillo, and M. Lone, "Aeroelastic damping estimation for a flexible high-aspect-ratio wing," *Journal of Aerospace Engineering*, vol. 35, no. 2, pp. 1–27, 2022.